



OPEN ACCESS

EDITED BY

Yi Xu,
Shanghai Jiao Tong University, China

REVIEWED BY

Hongzan Sun,
Shengjing Hospital of China Medical
University, China
Shengping Wang,
Fudan University, China
Shengdong Nie,
University of Shanghai for Science and
Technology, China

*CORRESPONDENCE

Zheng Yuan,
yuanzheng0404@163.com
Xiaoxiao Li,
jiayouxiaoxiao@163.com

[†]These authors have contributed equally
to this work and share first authorship

SPECIALTY SECTION

This article was submitted to Medical
Physics and Imaging,
a section of the journal
Frontiers in Physiology

RECEIVED 26 April 2022

ACCEPTED 13 July 2022

PUBLISHED 12 August 2022

CITATION

Shi H, Duan Y, Shi J, Zhang W, Liu W,
Shen B, Liu F, Mei X, Li X and Yuan Z
(2022), Role of preoperative prediction
of microvascular invasion in
hepatocellular carcinoma based on the
texture of FDG PET image: A
comparison of quantitative metabolic
parameters and MRI.
Front. Physiol. 13:928969.
doi: 10.3389/fphys.2022.928969

COPYRIGHT

© 2022 Shi, Duan, Shi, Zhang, Liu, Shen,
Liu, Mei, Li and Yuan. This is an open-
access article distributed under the
terms of the [Creative Commons
Attribution License \(CC BY\)](https://creativecommons.org/licenses/by/4.0/). The use,
distribution or reproduction in other
forums is permitted, provided the
original author(s) and the copyright
owner(s) are credited and that the
original publication in this journal is
cited, in accordance with accepted
academic practice. No use, distribution
or reproduction is permitted which does
not comply with these terms.

Role of preoperative prediction of microvascular invasion in hepatocellular carcinoma based on the texture of FDG PET image: A comparison of quantitative metabolic parameters and MRI

Huazheng Shi^{1†}, Ying Duan^{1†}, Jie Shi^{2†}, Wenrui Zhang¹,
Weiran Liu¹, Bixia Shen¹, Fufu Liu¹, Xin Mei¹, Xiaoxiao Li^{1*} and
Zheng Yuan^{3*}

¹Shanghai Universal Cloud Medical Imaging Diagnostic Center, Shanghai, China, ²Department of Hepatic Surgery VI, Eastern Hepatobiliary Surgery Hospital, The Second Military Medical University, Shanghai, China, ³Department of Radiology, Shanghai Ninth People's Hospital, Shanghai Jiao Tong University School of Medicine, Shanghai, China

Objective: To investigate the role of prediction microvascular invasion (mVI) in hepatocellular carcinoma (HCC) by ¹⁸F-FDG PET image texture analysis and hybrid criteria combining PET/CT and multi-parameter MRI.

Materials and methods: Ninety-seven patients with HCC who received the examinations of MRI and ¹⁸F-FDG PET/CT were retrospectively included in this study and were randomized into training and testing cohorts. The lesion image texture features of ¹⁸F-FDG PET were extracted using MaZda software. The optimal predictive texture features of mVI were selected, and the classification procedure was conducted. The predictive performance of mVI by radiomics classifier in training and testing cohorts was respectively recorded. Next, the hybrid model was developed by integrating the ¹⁸F-FDG PET image texture, metabolic parameters, and MRI parameters to predict mVI through logistic regression. Furthermore, the diagnostic performance of each time was recorded.

Results: The ¹⁸F-FDG PET image radiomics classifier showed good predicted performance in both training and testing cohorts to discriminate HCC with/without mVI, with an AUC of 0.917 (95% CI: 0.824–0.970) and 0.771 (95% CI: 0.578, 0.905). The hybrid model, which combines radiomics classifier, SUVmax, ADC, hypovascular arterial phase enhancement pattern on contrast-enhanced MRI, and non-smooth tumor margin, also yielded better predictive performance with an AUC of 0.996 (95% CI: 0.939, 1.000) and 0.953 (95% CI: 0.883, 1.000). The differences in AUCs between radiomics classifier and hybrid classifier were significant in both training and testing cohorts (DeLong test, both $p < 0.05$).

Conclusion: The radiomics classifier based on ^{18}F -FDG PET image texture and the hybrid classifier incorporating ^{18}F -FDG PET/CT and MRI yielded good predictive performance, which might provide a precise prediction of HCC mVI preoperatively.

KEYWORDS

hepatocellular carcinoma, microvascular invasion, fluorine-18 fluorodeoxyglucose-positron emission tomography (^{18}F -FDG-PET), magnetic resonance imaging, texture feature

1 Introduction

Hepatocellular carcinoma (HCC) is one of the most common liver malignancies and one of the leading causes of cancer death in the world (Sung et al., 2021). The main cause of unsatisfactory HCC prognosis is that it is difficult to detect at the early stage because of poor symptoms. The primary curative treatment modality of HCC is partial hepatectomy. However, upon detection, most HCC patients are unsuitable for hepatectomy because of the underlying liver cirrhosis and hepatic dysfunction. Even though HCC patients receive curative surgical resection, there is still a relatively high recurrence rate, even in HCC patients receiving liver transplantation, as high as 15%–30% (Hoffman and Mehta, 2021; Tampaki et al., 2021). Therefore, early diagnosis and accurate prediction of postoperative HCC recurrence are important. Some established factors such as tumor grade, stage, size, liver function, and treatment acted as predictors of postoperative HCC recurrence (Ochiai et al., 2012).

Vascular invasion of HCC representing invasive tumor behavior is a significant predictor of poor outcomes (Jonas et al., 2001). Macrovascular invasion (MVI) could be readily detected by contrast-enhanced CT/MR imaging before surgical resection (Teefey et al., 2003). However, as a histologic finding, microvascular invasion (mVI) is usually visible only on microscopy by histopathology of the surgical specimen, which is difficult to diagnose before surgical resection. Therefore, it is essential to detect clinical predictors to suggest the presence of mVI preoperatively.

Previous research has reported that the status of mVI can be predicted by key imaging and laboratory tests. Several previous studies have reported that tumor margin, capsule, and peritumoral enhancement on CT/MRI scans were significantly associated with mVI (Nishie et al., 2008; Witjes et al., 2012). However, contradictory results were also reported in some studies (Kim et al., 2009; Chou et al., 2014). In clinical practice, developing a reliable preoperative predictor for mVI is still necessary. As a functional molecular imaging modality, fluorine-18 fluorodeoxyglucose (^{18}F -FDG) positron emission tomography (PET)/computed tomography (CT) is useful for evaluating HCC differentiation grade by estimating the glucose metabolism of tumor cells (Cho et al., 2017). Recently, several studies have reported the role of ^{18}F -FDG PET/CT in defining mVI in patients with HCC. However, there is no

consistent conclusion, and the current results showed a wide range of sensitivity, specificity, and accuracy for preoperatively detecting mVI, which indicated that the current PET/CT technique is insufficient alone for establishing a risk factor for mVI (Kornberg et al., 2009; Lee et al., 2009; Lin et al., 2017; Kim and Kim, 2021). Recently, Li et al. conducted radiomics analysis on ^{18}F -FDG PET/CT to preoperatively predict mVI and prognosis in patients with very early and early stages of HCC, which is the importance of precise treatment of patients (Li et al., 2021).

In this retrospective study, we aimed to verify the comprehensive value of ^{18}F -FDG-PET/CT in the prediction of mVI by quantitative uptake measurement and image texture analysis. We also focus on the role of the hybrid model of incorporating ^{18}F -FDG-PET/CT and multi-parameter MRI. We hypothesized if ^{18}F -FDG-PET/CT findings predict mVI and, more importantly, the added value, if any, of PET/CT for the hybrid model in the prediction of mVI.

2 Materials and methods

2.1 Patients

This retrospective study was conducted in accordance with the Declaration of Helsinki proposed in 1975 and revised in 2000 and was approved by the Ethics Committee of the universal medical imaging center, Shanghai University (SHQJ-2019-05). The consecutive HCC patients were confirmed by histopathology after partial hepatectomy from January 2018 to April 2021. The inclusion criteria were as follows: (Sung et al., 2021) age >18 years; (Hoffman and Mehta, 2021) primary HCC confirmed by pathology of surgical specimens; (Tampaki et al., 2021) multi-parameter MR images containing conventional unenhanced MR imaging (including T1WI and T2WI), dynamic contrast-enhanced T1WI (including the arterial phase imaging, portal venous phase imaging, and delayed phase imaging), and diffusion-weighted imaging (DWI) (with b -value of 0 and 800 s/mm^2); (Ochiai et al., 2012) PET/CT and multi-parameter MRI examination approximately within 4 weeks before surgery; and (Jonas et al., 2001) no history of preoperative anti-cancer treatment. The exclusion criteria of this study were as follows: (Sung et al., 2021) preoperative

images showing macrovascular invasion; (Hoffman and Mehta, 2021) HCC patients who underwent any anti-cancer treatment before partial hepatectomy; (Tampaki et al., 2021) those with time intervals of PET/CT, MRI, and surgery more than 4 weeks; (Ochiai et al., 2012) those with no pathology slides available for review; and (Jonas et al., 2001) images with artifacts affecting evaluation.

The patients enrolled in this study were randomly divided into two cohorts (training and testing) with a ratio of 7:3 using computer-generated random numbers.

2.2 ¹⁸F-FDG PET/CT acquisition and image analysis

2.2.1 ¹⁸F-FDG PET/CT acquisition

This study examined all ¹⁸F-FDG PET/CT acquisitions with the SIEMENS Biograph mCT Flow PET/CT system (Siemens Medical Solutions United States, Inc.). After at least 6 h of fasting, the patient was intravenously administered a standard dose (3.7 MBq/kg) of ¹⁸F-FDG, followed by image acquisition 60 min later, from the thigh to the head. Whole-body non-contrast enhancement CT scanning protocols were as follows: 120 kVp, 30–170 mAs adjusted to the patient's body weight and with a section width of 3 mm and collimation of 0.75 mm. An emission scan was performed in a three-dimensional (3D) mode with an acquisition time of 1.7 min per bed position. PET images were reconstructed by a 2-iteration, 21-ordered-subset expectation maximization algorithm using CT images for attenuation correction.

2.2.2 ¹⁸F-FDG PET metabolic and volumetric parameters

Standardized uptake values (SUV) were calculated by the region-of-interest (ROI) technique. In order to calculate SUV_{max} and SUV_{mean}, manually defined circular ROI was drawn on attenuation-corrected emission images selected for the largest axial image of the HCC lesion. On the PET image, an ellipse iso-contour was drawn covering the lesion, and the volume of interest (VOI) in 3D, that is, metabolic tumor volume (MTV), was obtained semi-automatedly with an iso-contour SUV value threshold of 2.5 (Kim et al., 2017). Total lesion glycolysis (TLG) was calculated by multiplying the selected PET volume by the average SUV within that volume: TLG = MTV × (average SUV). If the lesion had a low uptake of ¹⁸F-FDG, the VOI was calculated on CT images and was then copied to PET to obtain the VOI on PET. Contrast-enhanced MRI was sometimes used to help delineate lesions.

The parameters of HCC ¹⁸F-FDG metabolic avidity SUV_{max}, SUV_{mean}, the ratio of the maximum standardized uptake value of tumor to the average standardized uptake value of normal liver (TLR_{max}), and the average tumor-to-normal liver standardized uptake value ratio (TLR_{mean}) were calculated and recorded.

2.2.3 Texture analysis on axial ¹⁸F-FDG PET images

2.2.3.1 Data standardization

Before texture analysis of the ¹⁸F-FDG PET image, the data standardization procession to minimize the influence of image contrast and brightness variations was performed by adopting a method of normalizing the intensities of greyscale images into the range of mean value ± three standard deviations (SD) ($\mu - 3SD, \mu + 3SD$).

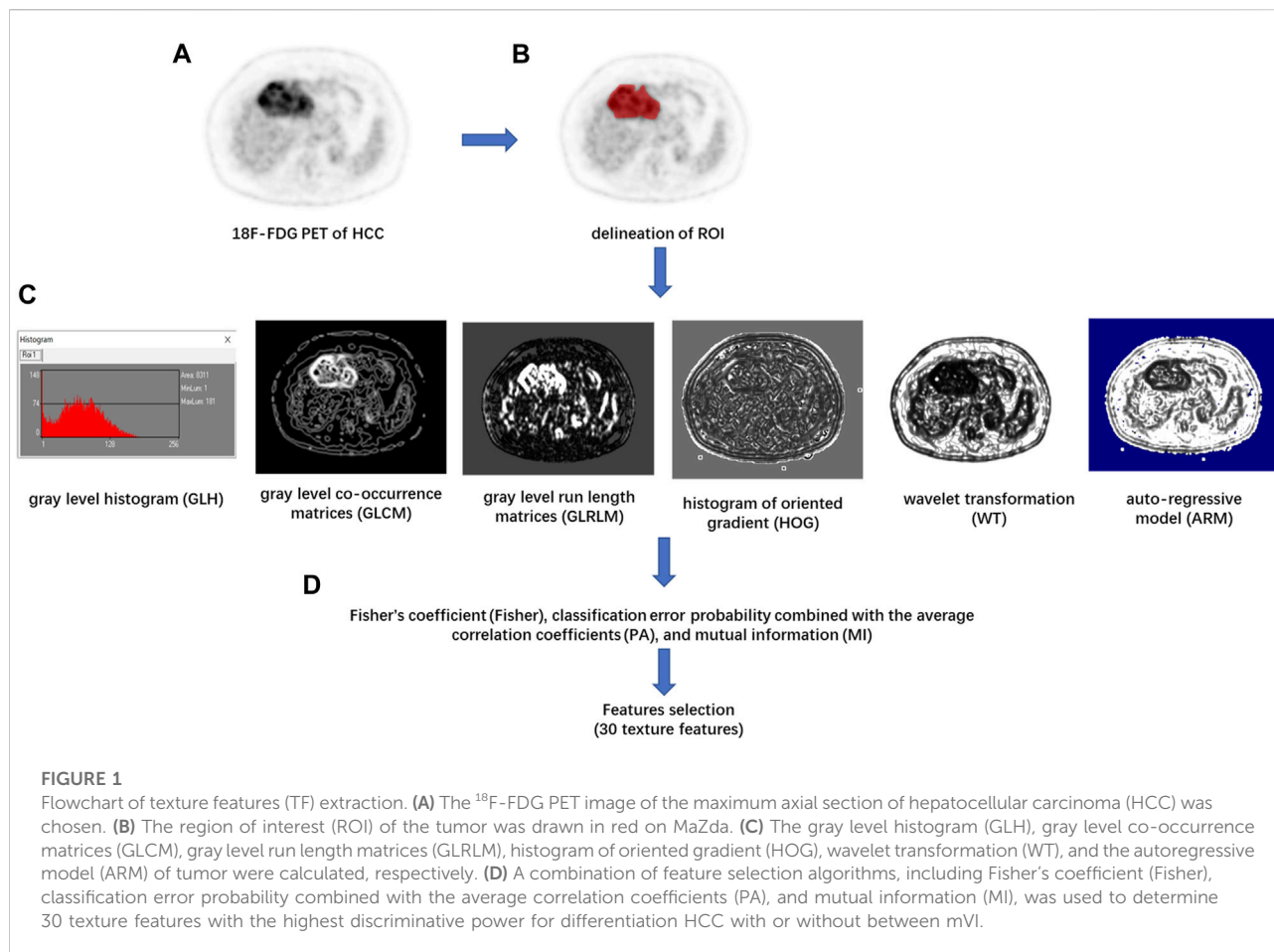
2.2.3.2 ¹⁸F-FDG PET image texture analysis

Texture feature extraction and selection were performed with the MaZda software package (version 4.6, available at <http://www.eletel.p.lodz.pl/mazda/>) (Szczyplinski et al., 2009). The largest axial ¹⁸F-FDG PET image of each HCC lesion was selected for image texture analysis. The ROI was manually circumscribed over the entire HCC lesion possibly on each selected image by an experienced radiologist (Figure 1). MaZda software allows the computation of almost 300 texture features based on the image histogram, co-occurrence matrix (COM), run-length matrix, absolute gradient, auto-regressive model, and wavelet transforms (WAV) (Pinker et al., 2018). These texture features (Supplementary Table S1) were extracted from each ROI.

In order to achieve the highest differentiation power of HCC with or without mVI, avoid the problem of dimensionality, and reduce the bias, the image texture feature selection was performed by a feature selection algorithm combining Fisher's coefficient (Fisher), classification error probability combined with the average correlation coefficients (PA), and mutual information (MI) on module B11. Then, 30 texture features with the highest discriminative power were selected. In the training cohort, the classification procedures were conducted using principal component analysis (PCA), linear discriminant analysis (LDA), and non-linear discriminant analysis (NDA) on module B11 of the MaZda software package, and the sensitivity, specificity, positive predictive value, negative predictive value, and accuracy of diagnosis were calculated. The best classification procedure was selected as the radiomic classifier with the highest accuracy. In the testing cohort, the optimal 30 texture features were selected according to the result of the training cohort, and the predictive performance of the radiomic classifier for differentiation of the status of mVI of HCC was calculated.

2.3 MRI technique and image analysis

All MRI examinations were performed with a 3.0-T MRI scanner (Magnetom Aera, Siemens Healthcare, Erlangen, Germany; or Ingenia, Philips Healthcare, Best, the Netherlands). The imaging protocol was as follows: axial fast spin echo T2WI with fat saturation using a navigator-triggered technique, DWI using a single-shot echoplanar imaging pulse sequence with *b*-values of



0 and 800 s/mm^2 . The apparent diffusion coefficient (ADC) of the HCC lesion was measured on the ADC map by the ROI drawn by two radiologists circumscribing the entire lesion on the largest axial image in consensus. T1WI images were obtained before and after administration of gadolinium injection solution, with a dose of 0.1 mmol per kilogram of body weight and an injection rate of 2 ml/sec. The arterial phase (AP) images were acquired approximately 25 s after contrast material injection. The portal venous phase (PVP) images were acquired approximately 55–65 s after the start of contrast material administration, and delayed phase (DP) images were acquired 90–100 s after contrast material injection. All parameters for the MRI sequences are summarized in [Supplementary Table S2](#).

2.3.1 Image analysis

MR images were retrospectively analyzed on a workstation or a picture archiving and communication system (PACS). Two clinically experienced radiologists evaluated the MR images in consensus to obtain reliable results. Both readers were blinded to the status of mVI.

The two radiologists qualitatively made the following: 1) classified the arterial phase enhancement patterns on dynamic

contrast-enhanced MRI into three patterns: hypervascular HCC, isovascular HCC, and hypovascular HCC; ([Hoffman and Mehta, 2021](#)) determined the presence or absence of intratumoral artery; 2) classified the patterns of tumor margin into two patterns: smooth margin or non-smooth margin; and 3) determined HCC with or without peritumoral enhancement on the AP images.

Qualitative findings on dynamic contrast-enhanced MR imaging were defined as follows: 1) hypervascular HCC: homogeneously hypervascular, hypervascular with slit-like hypovascular foci, or multifocal hypovascular foci, with a peripheral hypovascular area ([Figure 2](#)); 2) hypovascular HCC: with a nodular- or irregular-shaped hypointense portion at an inner area, with irregular rim-like enhancement, with a peripheral hypervascular area, discontinuous rim, or crescent-like, with linear or spot-like hypervascular foci, or completely hypovascular HCC ([Figure 2](#)) ([Rhee et al., 2021](#)); 3) intratumoral artery: the blood vessels within the tumor in AP images ([Figure 2](#)) ([Segal et al., 2007](#)); 4) a smooth margin defined as a nodular-shaped tumor without extranodular extension or infiltrative, non-smooth margins defined as a nodule with extranodular extension or an infiltrative margin ([Figure 3](#)) ([Nakashima et al., 2003](#); [Segal et al., 2007](#)); and 5)

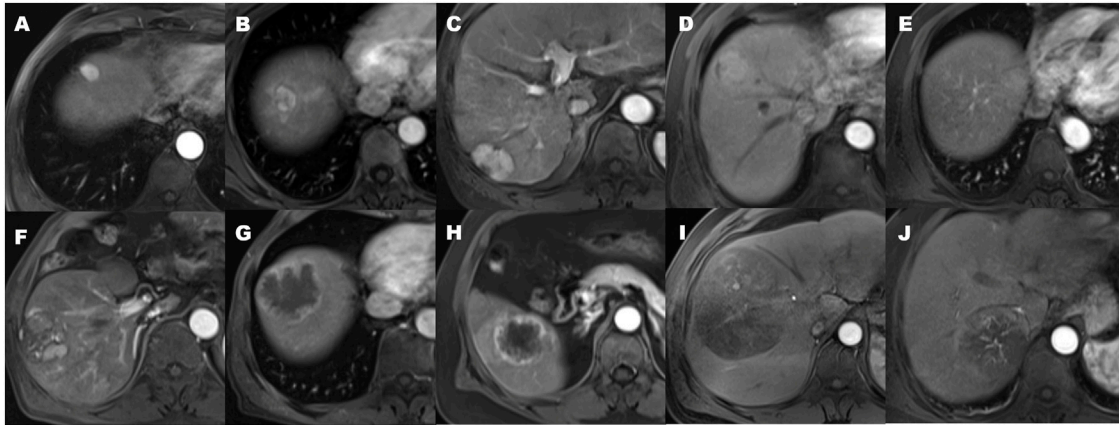


FIGURE 2

The patterns of arterial phase enhancement of hepatocellular carcinoma on contrast-enhanced MRI. **(A)** Homogeneously hypervascular HCC. **(B)** Hypervascular HCC with slit-like hypovascular foci. **(C)** With multifocal hypovascular foci. **(D)** Hypervascular HCC with the peripheral hypovascular area. **(E)** Completely isovascular HCC. **(F)** HCC with a nodular or irregular-shaped hypovascular portion at the inner area. **(G)** Hypovascular HCC with irregular rim-like enhancement. **(H)** Hypovascular HCC with the peripheral hypervascular area, discontinuous rim or crescent-like, and the presence of peritumoral enhancement seen in the arterial phase. **(I)** Hypovascular HCC with linear or spot-like hypervascular foci. **(J)** the presence of an intratumoral artery.

peritumoural enhancement on AP images: defined as a patchy hyperintense area adjacent to the tumor with broad contact to the tumor border on the AP images, presenting isointense to liver parenchyma on the DP images (Figure 2) (Kim et al., 2009).

2.4 Intra-observer and inter-observer agreement

The reproducibility of the intra-observer and inter-observer agreement for texture analysis was measured using 20 randomly chosen samples drawn from axial ^{18}F -FDG PET images and ADC map by two radiologists blinded from patients' characteristics. To evaluate intra-observer reproducibility, the first radiologist delineated an ROI twice within 2 weeks following the same procedure. Meanwhile, the second radiologist also independently delineated the ROI once following the same procedure. Then, the inter-observer agreement was assessed by comparing the results with the texture features extracted calculated from the first ROI delineation by the first radiologist. The intraclass correlation coefficient (ICC) was used to evaluate the intra-observer and inter-observer agreements. An ICC >0.75 indicated satisfactory agreement.

2.5 Microvascular invasion evaluation by histopathology

All surgical specimens and the status of mVI were reviewed and evaluated by an experienced pathologist in liver pathology.

mVI was defined as the presence of a tumor in a portal vein, hepatic vein, or a large capsular vessel of the surrounding hepatic tissue lined by the endothelium that was visible only on microscopy (Roayaie et al., 2009; Xu et al., 2019). We categorized the HCC patients with mVI as the mVI-positive (mVI+) group and the HCC patients without mVI as the mVI negative (mVI-) group.

2.6 Statistical analysis

Inter-reader agreement was expressed by Cohen's kappa coefficient. A kappa statistic of 0.8–1.0, 0.6–0.79, 0.40–0.59, 0.2–0.39, and 0–0.19 was considered excellent, good, moderate, fair, and poor agreement, respectively.

For categorical variables, the differences between the mVI (-) and mVI (+) groups were analyzed by the Chi-squared test or Fisher's exact test. For continuous variables with a normal distribution, an independent-samples *t*-test was used to test the significant difference of the mVI (-) and mVI (+) groups; for continuous variables with a skewed distribution, a non-parametric Mann-Whitney *U* test was used. A two-tailed *p*-value less than 0.05 was considered that the difference was statistically significant. SPSS software (SPSS version 24.0; SPSS Inc., Chicago, IL, United States) was used to perform statistical analysis. The predictive value of each factor for mVI was determined by analysis of the area under the ROC curve (AUC). The differences in AUCs were compared by the DeLong test (DeLong et al., 1988) performed using MedCalc software (version 20.023). The calibration of the hybrid model

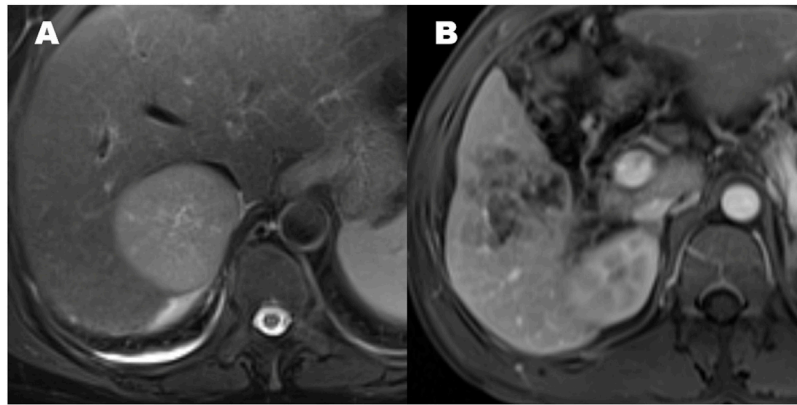


FIGURE 3

The patterns of hepatocellular carcinoma tumor margin. (A) Smooth tumor margin and intact tumor capsule. (B) Tumor with a non-smooth margin.

was performed by comparing the predicted and actual probability of mVI by the Hosmer–Lemeshow test.

3 Results

For the intra-observer and inter-observer agreement, radiomics features achieved satisfactory consistency. There was no radiomics feature to be eliminated. The mean ICC was 0.956 (range, 0.892 to 1, $p < 0.001$) in the intra-observer agreement and the mean ICC was 0.915 (range, 0.751 to 0.999, $p < 0.001$) in the inter-observer agreement.

In this study, the study flowchart for predicting mVI based on texture features, metabolic and volumetric parameters, and multi-parameter MRI is shown in [Figure 4](#). A total of 97 patients' clinical characteristics are presented in [Table 1](#).

Of the 97 patients with HCC, 58.8% (57/97) had tumors with mVI and 41.2% (40/97) without mVI. In the training cohort, mVI (+) was presented in 55.9% (38/68) of tumors, similar to 65.5% (19/29) seen in the testing cohort ($p > 0.05$). There were also no significant differences in other baseline clinical features between the training and testing groups (all $p > 0.05$, [Table 1](#)), which indicated that the distribution of baseline clinical-pathologic characteristics in the training and testing group was balanced.

In the pooled cohorts, the values of SUVmax, SUVmean, TLRmax, TLRmean, and ADC of HCC with mVI ($n = 57$) were higher than HCC without mVI ($n = 40$) (all $p < 0.05$). There was no significant difference in MTV, TLG, and ADC/ADC_liver between HCC with and without mVI ([Table 2](#); [Figures 5, 6](#)).

ROC curve analysis showed that the cutoff values of SUVmax, SUVmean, TLRmax, TLRmean, and ADC for predicting HCC with mVI were 5.65, 3.79, 2.53, 1.92, and

1,171.5, respectively, with the largest Youden indexes but moderate diagnostic efficacy (all AUC < 0.70) ([Table 3](#)). In all quantitative metabolic parameters, the predictor with the highest diagnostic efficacy is SUVmax with the largest AUC (0.698, 95% CI: 0.593 to 0.803, $p = 0.001$), providing sensitivity and specificity of 59.6% and 80.0% at a cutoff value of 5.65 ([Table 4](#); [Supplementary Figure S1](#)).

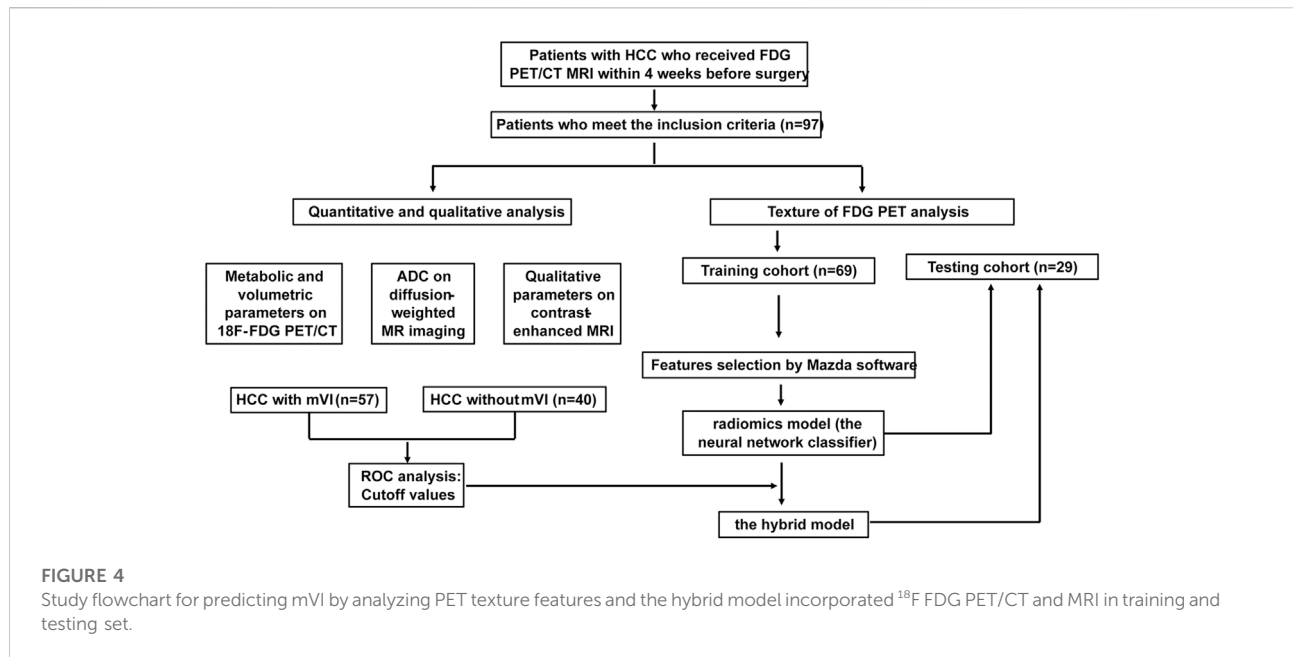
On dynamic contrast-enhanced MRI review of pooled all cohorts, the HCCs with mVI were significantly associated with enhancement patterns on AP imaging and tumor margin (all $p < 0.05$; [Table 2](#)). Most HCCs with mVI (44/57, 77.2%) demonstrated hypovascular lesions ([Figure 5](#)). The HCCs with mVI (28/57, 49.1%) manifest as having more frequency of non-smooth tumor margin than the HCCs without mVI (11/40, 27.5%).

Based on the above results, we selected the quantitative parameters of SUVmax and ADC, as well as the qualitative parameters of the hypovascular enhancement pattern on AP MR imaging and non-smooth tumor margin for subsequent analysis.

3.1 Training cohort

Based on the feature selection algorithm combining Fisher, PA, and MI coefficients in features modeling, 30 optimal features are selected and listed in [Supplementary Table S3](#).

Compared to PCA (47.1%, 32/68) and LDA (19.1%, 13/68), NDA had the lowest misclassification rate with 7.4% (5/68) for all these three classification procedures by MaZda software ($p < 0.01$). The NDA classification with an AUC of 0.917 (95% CI: 0.824–0.970) showed a sensitivity of 100%, a specificity of 83.3%, a positive predictive value of 88.4%, a negative predictive value of 100%, and an accuracy of 92.6% ([Table 4](#)).



Combining radiomics classification results based on the texture of the ¹⁸F-FDG-PET image, SUVmax, ADC, and the qualitative parameters of the hypovascular arterial phase enhancement pattern and non-smooth tumor margin, the hybrid model regression equation was as follows:

$$\text{Logit}(P) = -2.077 + 0.203 \times \text{SUVmax} + 2.825 \times \text{ADC} - 4.717 \times \text{Radiomics} - 0.041 \times \text{non-smooth} - 0.664 \times \text{hypovascular}.$$

P is the probability of HCC with mVI. For $p \geq 0.5$, the lesion was expected to be HCC with mVI, whereas the other lesions were categorized as HCC without mVI.

The hybrid model with an AUC of 0.996 (95% CI: 0.939, 1.000; $p < 0.001$) yielded a sensitivity of 94.7%, a specificity of 100%, a positive predictive value of 100%, a negative predictive value of 93.8%, and an accuracy of 97.1% (Table 4). The difference in AUC between the radiomics classification model and the hybrid model was significant ($p = 0.017$). The calibration of the hybrid model was performed by comparing the predicted and actual probability of mVI by the Hosmer–Lemeshow test ($p > 0.05$). (Supplementary Figure S2A) The difference between the predicted and actual probabilities of mVI showed no statistical significance.

3.2 Testing cohort

We selected 30 texture features that were consistent with the training cohort. By using the neural network NDA classifier test included in module B11, the misclassification rate for HCC with

versus without mVI was 20.7% (6/29). The sensitivity, specificity, positive predictive, negative predictive, and accuracy values were 84.2%, 70.0%, 84.2%, 70.0%, and 79.3%, respectively, with an AUC of 0.771 (95% CI: 0.578, 0.905) (Table 4).

In the testing cohort, the hybrid criteria yielded an AUC of 0.953 (95% CI: 0.883, 1.000; $p < 0.001$), a sensitivity of 95.0%, a specificity of 70%, a positive predictive value of 86.4%, a negative predictive value of 87.5%, and an accuracy of 86.7% (Table 4).

The performances of the radiomics and hybrid models to predict HCC with mVI were also good in the testing cohort, indicating their robustness. The difference in AUC between radiomics criteria and hybrid criteria was also significant ($p = 0.013$), indicating that the hybrid model incorporated ¹⁸F-FDG PET/CT and MRI yielded better predictive performance. The calibration of the hybrid model was performed by comparing the predicted and actual probability of mVI by the Hosmer–Lemeshow test ($p > 0.05$) (Supplementary Figure S2B). The difference between the predicted and actual probability of mVI showed no statistical significance.

4 Discussion

To our knowledge, this study has produced the first texture-based radiomics model of ¹⁸F FDG PET and a hybrid model that incorporated texture features of ¹⁸F-FDG PET, quantitative metabolic parameters, and quantitative and qualitative MRI parameters for predicting the status of mVI in HCC. We found that the radiomics model based on the texture of ¹⁸F-FDG PET had a good diagnostic performance with an

TABLE 1 Clinical characteristics of patients with HCC in the training and testing cohort.

	Training cohort (<i>n</i> = 68)			Testing cohort (<i>n</i> = 29)			<i>p</i> -value***
	mVI+ (<i>n</i> = 38) <i>n</i> (%) or median (IQR)	mVI- (<i>n</i> = 30) <i>n</i> (%) or median (IQR)	<i>p</i> -value*	mVI+ (<i>n</i> = 19) <i>n</i> (%) or median (IQR)	mVI- (10) <i>n</i> (%) or median (IQR)	<i>p</i> -value**	
Sex			0.452			0.414	0.519
	Male	26 (38.2)	23 (33.8)	11 (37.9)	8 (27.6)		
	Female	12 (17.6)	7 (10.3)	8 (27.6)	2 (6.9)		
Age (years)		55 (36.5, 59.3)	55 (50, 63.3)	50 (50, 62)	46 (55, 62)	0.628	0.512
HBV infection			0.965			0.450	0.583
	Absent	15 (22.1)	12 (17.6)	11 (37.9)	4 (13.8)		
	Present	23 (33.8)	18 (26.5)	8 (27.6)	6 (20.7)		
Child-Pugh			0.973			1.000	0.961
	A	29 (42.6)	23 (33.8)	14 (48.3)	7 (24.1)		
	B	9 (13.2)	7 (10.3)	5 (17.2)	3 (10.3)		
Liver cirrhosis			0.833			0.245	0.420
	Absent	13 (19.1)	11 (16.2)	8 (27.6)	7 (24.1)		
	Present	25 (36.8)	19 (27.9)	11 (37.9)	3 (10.3)		
AFP (ng/ml)			0.357			0.270	0.932
	≤200	16 (23.5)	16 (23.5)	12 (41.4)	4 (13.8)		
	>200	22 (32.3)	14 (20.6)	7 (24.1)	6 (20.7)		
Image tumor size (mm)		42 (18.8, 79.3)	40 (17.5, 69.8)	64.0 (55.0, 85.0)	67.5 (44.0, 96.3)	0.982	0.888

HCC, hepatocellular carcinoma; HBV, hepatitis B virus; AFP, alpha-fetoprotein; mVI, microvascular invasion; IQR, interquartile range.

*The difference in HCC with mVI and without mVI in the training cohort.

**The difference in HCC with mVI and without mVI in the testing cohort.

***The difference in HCC with mVI and without mVI in the pooled cohort.

AUC of 0.917 (95% CI: 0.836–0.998) and 0.771 (95% CI: 0.578 TO 0.966) in the training and testing cohorts, respectively. Furthermore, hybrid criteria combining ¹⁸F-FDG PET and MRI could significantly increase diagnostic performance more than the radiomics model ($p < 0.05$) and yield an AUC of 0.996 (95% CI: 0.939, 1.000; $p < 0.001$) and 0.953 (95% CI: 0.883, 1.000) in the training and testing cohorts, respectively. Accordingly, our results may increase the accuracy of preoperative detection of the HCC with or without mVI. It is useful for planning the most appropriate treatment strategy and improving the prognosis of patients with HCC.

Despite progressions in diagnostic and therapeutic modalities, the prognosis of the patient with HCC is still to be improved due to the recurrence rate after treatment remaining high (Mlynarsky et al., 2015). The high heterogeneity of the HCC may have resulted in a varied prognosis (Lu et al., 2016; Lin et al., 2017). As a pathological feature, mVI reflects the invasiveness of the tumor, which usually appears in aggressive HCC while not in low-grade HCC. The patient with HCC presenting mVI has a shorter disease-free survival (DFS) due to a higher risk of

tumor recurrence (Miyata et al., 2006). Therefore, mVI is an important prognostic factor of HCC and plays an important role in planning a personalized therapeutic strategy (Erstad and Tanabe, 2019; Xu et al., 2019). It is necessary to detect clinical predictors to suggest the presence of mVI preoperatively in order to establish a personalized therapeutic strategy.

Several previous studies have shown that various imaging modalities, including ultrasound, CT, especially contrast-enhanced CT, ¹⁸F-FDG PET/CT, and MRI, have the potential to detect HCC with mVI (Lin et al., 2017; Hyun et al., 2018; Hu et al., 2019; Li et al., 2021; Meng et al., 2021). These studies showed that various imaging modalities might have a comparable predictive performance for mVI, whether the morphologic features, metabolic activity features, radiomics analysis, or combination are used. However, it is still unclear which modality is better and unable to completely meet clinical needs to establish risk factor for mVI only by one modality. In this study, we first extracted texture features from ROI in an ¹⁸F-FDG PET image and selected 30 optimal texture features in our study. Meanwhile, the NDA classification procedure and the neural network classifier on module B11 of the MaZda software

TABLE 2 Radiologic findings of primary HCC in the training and testing cohorts.

	Training cohort (n = 68)			Testing cohort (n = 29)			p-value***
	mVI+ (n = 38) n (%) or median (IQR)	mVI- (n = 30) n (%) or median (IQR)	p value*	mVI+ (n = 19) n (%) or median (IQR)	mVI- (10) n (%) or median (IQR)	p-value**	
SUVmax			0.056			0.068	0.011
	6.2 (3.9, 8.3)	4.0 (2.6, 4.8)		7.8 (4.0, 9.3)	4.5 (2.6, 8.2)		
SUVmean			0.022			0.211	0.006
	4.2 (2.6, 5.6)	3.0 (2.1, 3.3)		4.7 (2.9, 6.6)	3.4 (2.4, 5.8)		
TLRmax			0.006 ^a			0.153	0.001 ^a
	3.1 (2.3, 4.7)	2.1 (1.7, 2.5)		4.0 (2.0, 6.4)	2.6 (1.5, 4.7)		
TLRmean			0.029 ^a			0.338	0.017 ^a
	2.4 (1.4, 3.2)	1.6 (1.3, 1.8)		2.5 (1.5, 4.3)	1.8 (1.5, 3.4)		
MTV			0.168			0.737	0.303
	33.0 (6.7,141.3)	15.9 (5.8, 104.9)		101.2 (18.5, 180.8)	81.5 (8.3, 241.2)		
TLG			0.155 ^a			0.728	0.102
	115.0 (22.6, 940.2)	48.1 (13.2, 350.4)		661.3 (70.4, 1,507.2)	255.5 (31.4, 1728.2)		
ADC (×10 ⁻³ mm ² /s)			0.091			0.066	0.014
	1.29 (1.07, 1.42)	1.12 (0.94, 1.25)		1.19 (0.87, 1.54)	1.03 (0.83, 1.25)		
ADC/ADC_liver			0.365			0.945 ^a	0.650 ^a
	0.9 (0.8, 1.3)	1.0 (0.9, 1.2)		1.3 (1.0, 1.7)	1.1 (1.0, 1.8)		
Arterial phase enhancement pattern		<0.001			0.698	<0.001	
Hypervascular	7 (10.3)	19 (27.9)		6 (20.7)	4 (13.8)		
Hypovascular	31 (45.6)	11 (16.2)		13 (44.8)	6 (20.7)		
Intratumoral artery		1.000			0.372	0.642	
Presence	5 (7.4)	4 (5.9)		3 (10.3)	3 (10.3)		
Absence	33 (48.5)	26 (38.2)		16 (55.2)	7 (24.1)		
Tumor margin		0.053			0.694	0.033	
Smooth	22 (32.4)	24 (35.3)		7 (24.1)	5 (17.2)		
Non-smooth	16 (23.5)	6 (8.8)		12 (41.4)	5 (17.2)		
Peritumoral enhancement in the arterial phase		0.204			0.449	0.077	
Presence	10 (14.7)	5 (7.4)		9 (31.0)	3 (10.3)		
Absence	28 (41.2)	25 (36.8)		10 (34.5)	7 (24.1)		

HCC, hepatocellular carcinoma; mVI, microvascular invasion; IQR, interquartile range; TLRmax, SUVmax/SUVmen_liver; TLRmean, SUVmean/SUVmen_liver; MTV, metabolic tumor volume; TLG, total lesion glycolysis; ADC, apparent diffusion coefficient.

*The difference in HCC with mVI and without mVI in the training cohort.

**The difference in HCC with mVI and without mVI in the testing cohort.

***The difference in HCC with mVI and without mVI in the pooled cohort.

^aNon-parametric Mann-Whitney *U* test.

package were adopted to construct a radiomics model for predicting HCC with mVI. Our results showed that the radiomics model derived from the image texture feature of axial ¹⁸F-FDG PET achieved a classification accuracy of 92.6% with an AUC of 0.917 in the training cohort and 79.3% with an AUC of 0.771 in the testing cohort. However, the traditional imaging radiologic features or metabolic activity features, such as

quantitative metabolic parameters from PET/CT or quantitative and qualitative MRI parameters, yielded an accuracy range from 58.8% to 73.5% in the training cohort and 58.6%–72.4% in the testing cohort. These results showed that the radiomics model may be much better than the traditional morphologic and metabolic activity features. A recent study showed that a radiomics nomogram based on ¹⁸F-FDG PET/CT was constructed to

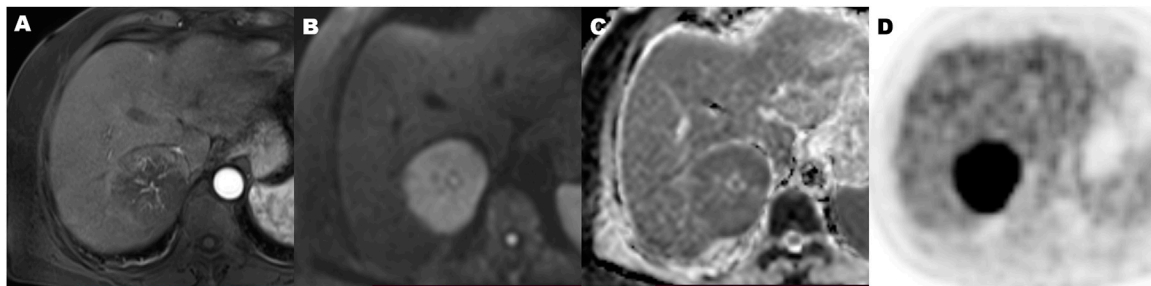


FIGURE 5

A 70-year-old hepatocellular carcinoma in liver segment VII woman with microvascular invasion, demonstrating Hypovascular enhancement pattern, high metabolic of SUVmax 9.2, MTV 134.2 cm³, TLG 915.2, TLR 4.5, and ADC of 0.86×10^{-3} mm²/s. Contrast-enhanced MR in arterial phase image (A), diffusion-weighted MR image (B), ADC map (C), and ¹⁸F-FDG PET (D) (MTV, metabolic tumor volume; TLG, total lesion glycolysis; TLR, ratio of tumor-to-liver SUV; ADC, apparent diffusion coefficient).

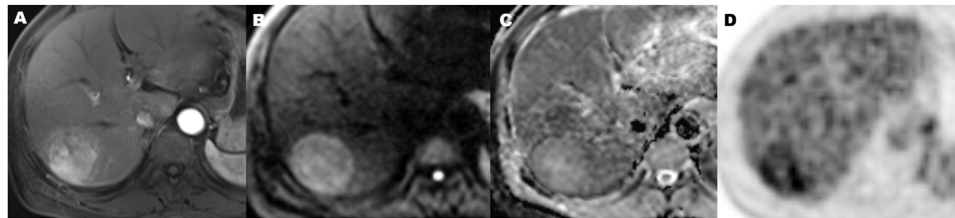


FIGURE 6

A 56-year-old hepatocellular carcinoma in liver segment VII man without microvascular invasion, demonstrating hypervascular enhancement pattern, low metabolic of SUVmax 3.5, MTV 72.2 cm³, TLG 196.5, TLR 1.9, and ADC value of 1.1×10^{-3} mm²/s. Contrast-enhanced MR in arterial phase image (A), diffusion-weighted MR image (B), ADC map (C), and ¹⁸F-FDG PET (D) (MTV, metabolic tumor volume; TLG, total lesion glycolysis; TLR, ratio of tumor-to-liver SUV; ADC, apparent diffusion coefficient).

TABLE 3 ROC results of ¹⁸F-FDG PET/CT parameters and ADC in predicting HCC with mVI in the pooled cohort.

Characteristic parameter	Area under curve	p-values	Sensitivity (%)	Specificity (%)	Cutoff
SUVmax	0.698 (0.593, 0.803)	0.001	59.6	80.0	5.65
SUVmean	0.676 (0.567, 0.786)	0.003	66.7	77.5	3.79
TLRmax	0.693 (0.586, 0.799)	0.001	68.4	70.0	2.53
TLRmean	0.643 (0.531, 0.756)	0.017	64.9	75.0	1.92
ADC($\times 10^{-3}$ mm ² /s)	0.651 (0.537, 0.765)	0.012	68.4	75.0	1.17

ROC, receiver operating-characteristic curve; HCC, hepatocellular carcinoma; mVI, microvascular invasion; TLRmax, SUVmax/SUVmen_{liver}; TLRmean, SUVmean/SUVmen_{liver}; ADC, apparent diffusion coefficient.

predict the mVI status in patients with very-early- and early-stage HCC with an AUC of 0.891 (95% CI: 0.799–0.984) in the training cohort and an AUC of 0.692 (95% CI: 0.497–0.887) in the testing cohort, which also showed that the radiomics model had a strong predictive power in detecting HCC with mVI (Li et al., 2021).

Of course, there are still several remaining significant challenges for radiomics in detecting HCC with mVI, such as

replicability, standardization of images and data, and ethical and regulatory considerations (Forghani et al., 2019). In our study, we adopted a method of normalizing image intensities in the range of mean gray-level value \pm three standard deviations (SD) to minimize the influence of contrast and brightness variation. In the testing cohort, our radiomics criteria yielded a classification accuracy of 79.3% with an

TABLE 4 Diagnostic performance of hepatocellular carcinoma with microvascular invasion in the training and testing cohorts.

	True positive	False positive	False negative	True negative	Sensitivity	Specificity	Positive-predictive value	Negative-predictive value	Accuracy
Training cohort (<i>n</i> = 68)									
Radiomics model	38	5	0	25	100	83.3	88.4	100	92.6%
SUVmax	20	5	18	25	52.6	83.3	80	58.1	66.2
ADC	26	8	12	22	68.4	73.3	76.5	64.7	70.6
Hypovascular	31	11	7	19	81.6	63.3	73.8	73.1	73.5
Non-smooth margin	16	6	22	24	42.1	80	72.7	52.2	58.8
Hybrid model	36	0	2	30	94.7	100	100	93.8	97.1
Testing cohorts (<i>n</i> = 29)									
Radiomics model	16	3	3	7	84.2	70	84.2	70	79.3
SUVmax	14	3	5	7	73.7	70	82.4	58.3	72.4
ADC	13	6	2	8	86.7	57.1	68.4	80	72.4
Hypovascular	13	6	6	4	68.4	40	68.4	40	58.6
Non-smooth margin	12	5	7	5	63.2	50	70.6	41.7	58.6
Hybrid model	19	3	1	7	95	70	86.4	87.5	86.7

AUC of 0.771 (95% CI: 0.578–0.905), which was lower than that classification accuracy of 92.6% with an AUC of 0.917 (95% CI: 0.824–0.970) in the training cohort. This indicated that the robustness of radiomics was to be improved.

The previous studies have also reported that the quantitative and qualitative parameters of SUVmax, ADC values, hypovascular lesion, and non-smooth tumor margin were associated with mVI status in patients with HCC (Mulé et al., 2020; Zhang et al., 2020). Therefore, in this study, we constructed hybrid criteria combining radiomics criteria and quantitative and qualitative parameters derived from ¹⁸F-FDG PET/CT and MRI to predict the status of mVI in patients with HCC and achieved better results by significantly increasing AUC, yielded an AUC of 0.996 (95% CI: 0.939 to 1.000; *p* < 0.001) and 0.953 (95% CI: 0.883–1.000) in the training and testing cohorts, respectively. The difference in AUC between hybrid criteria and radiomics criteria showed statistical significance (*p*-values of 0.0165 and 0.0133 in the training and testing cohorts, respectively). Our findings suggest that the utility of the hybrid model combining ¹⁸F-FDG PET/CT and MRI may improve the preoperative prediction of the status of mVI in HCC, compared to the only utility of the radiomics model based on texture features of ¹⁸F-FDG PET.

There were several limitations in this study. First, this was a retrospective study with a small sample size, which could influence the robustness and reproducibility of our prediction models. The study samples were only divided into the training and testing cohorts to perform internal validation in this study. There may be a phenomenon of

overfitting in the data processing for the AUC significant difference between the radiomics classifier training set and the validation set. Therefore, the current study should need further validation with data augmentation and cross-validation in the future. Second, in this study, the HCC ¹⁸F-FDG PET image textures were extracted only from the two-dimensional largest axial image of each HCC, which may cause loss of the entire tumor heterogeneity information. Therefore, the 3D structures radiomics of the tumor need further study in the future. Third, there was no significant association between the clinical characteristics and the status of mVI in our study (*p* > 0.05). It was different from the previous study by Hyun et al. (2018), which showed that some clinical characteristics of clinical stage, AST, and AFP were significant predictors of mVI. The radiological hybrid model incorporating more clinical, pathological, and prognosis characteristics and radiomics should be considered in future studies.

In conclusion, the hybrid radiological model that incorporates the image texture of the ¹⁸F-FDG PET signature, quantitative metabolic parameter, and quantitative and qualitative MRI parameters has powerful predictive performance in predicting the status of mVI preoperatively. Thus, such models may facilitate planning clinical treatment and improving survival in selected patients with HCC. Of course, it is warranted to validate the robustness and reproducibility of our prediction models by large-scale multicenter studies in the future.

Data availability statement

The raw data supporting the conclusions of this article will be made available by the authors without undue reservation.

Ethics statement

The studies involving human participants were reviewed and approved by the Ethics Committee of the universal medical imaging center, Shanghai University. Written informed consent for participation was not required for this study in accordance with the national legislation and the institutional requirements.

Author contributions

The literature search, analysis, data explanation, and manuscript draft were finished by HS, XL, and ZY. XL and ZY are responsible for the analysis and explanation of the radiomics imaging features data. YD, JS, WZ, WL, BS, FL, and XM acquired the clinical information and imaging. HS and ZY designed the study, explained the data, and made multiple revisions to the manuscript. All authors contributed to the article and approved the submitted version.

References

- Cho, K. J., Choi, N. K., Shin, M. H., and Chong, A. R. (2017). Clinical usefulness of FDG-PET in patients with hepatocellular carcinoma undergoing surgical resection. *Ann. Hepatobiliary. Pancreat. Surg.* 21, 194–198. doi:10.14701/ahbps.2017.21.4.194
- Chou, C. T., Chen, R. C., Lin, W. C., Ko, C. J., Chen, C. B., Chen, Y. L., et al. (2014). Prediction of microvascular invasion of hepatocellular carcinoma: preoperative CT and histopathologic correlation. *AJR. Am. J. Roentgenol.* 203, W253–W259. doi:10.2214/AJR.13.10595
- DeLong, E. R., DeLong, D. M., and Clarke-Pearson, D. L. (1988). Comparing the areas under two or more correlated receiver operating characteristic curves: a nonparametric approach. *Biometrics* 44, 837. doi:10.2307/2531595
- Erstad, D. J., and Tanabe, K. K. (2019). Prognostic and therapeutic implications of microvascular invasion in hepatocellular carcinoma. *Ann. Surg. Oncol.* 26, 1474–1493. doi:10.1245/s10434-019-07227-9
- Forghani, R., Savadjiev, P., Chatterjee, A., Muthukrishnan, N., Reinhold, C., Forghani, B., et al. (2019). Radiomics and artificial intelligence for biomarker and prediction model development in oncology. *Comput. Struct. Biotechnol. J.* 17, 995–1008. doi:10.1016/j.csbj.2019.07.001
- Hoffman, D., and Mehta, N. (2021). Recurrence of hepatocellular carcinoma following liver transplantation. *Expert Rev. Gastroenterol. Hepatol.* 15, 91–102. doi:10.1080/17474124.2021.1823213
- Hu, H. T., Wang, Z., Huang, X. W., Chen, S. L., Zheng, X., Ruan, S. M., et al. (2019). Ultrasound-based radiomics score: a potential biomarker for the prediction of microvascular invasion in hepatocellular carcinoma. *Eur. Radiol.* 29, 2890–2901. doi:10.1007/s00330-018-5797-0
- Hyun, S. H., Eo, J. S., Song, B. I., Lee, J. W., Na, S. J., Hong, I. K., et al. (2018). Preoperative prediction of microvascular invasion of hepatocellular carcinoma using (18)F-FDG PET/CT: a multicenter retrospective cohort study. *Eur. J. Nucl. Med. Mol. Imaging* 45, 720–726. doi:10.1007/s00259-017-3880-4
- Jonas, S., Bechstein, W. O., Steinmuller, T., Herrmann, M., Radke, C., Berg, T., et al. (2001). Vascular invasion and histopathologic grading determine outcome

Funding

This work was supported by the Shanghai Municipal Health Commission (No. 20194Y0148) and the National Natural Science Foundation of China (No. 82073293).

Conflict of interest

The authors declare that the research was conducted in the absence of any commercial or financial relationships that could be construed as a potential conflict of interest.

Publisher's note

All claims expressed in this article are solely those of the authors and do not necessarily represent those of their affiliated organizations or those of the publisher, the editors, and the reviewers. Any product that may be evaluated in this article, or claim that may be made by its manufacturer, is not guaranteed or endorsed by the publisher.

Supplementary material

The Supplementary Material for this article can be found online at: <https://www.frontiersin.org/articles/10.3389/fphys.2022.928969/full#supplementary-material>

after liver transplantation for hepatocellular carcinoma in cirrhosis. *Hepatology* 33, 1080–1086. doi:10.1053/jhep.2001.23561

Kim, H., Park, M. S., Choi, J. Y., Park, Y. N., Kim, M. J., Kim, K. S., et al. (2009). Can microvessel invasion of hepatocellular carcinoma be predicted by pre-operative MRI? *Eur. Radiol.* 19, 1744–1751. doi:10.1007/s00330-009-1331-8

Kim, K., and Kim, S. J. (2021). Diagnostic test accuracies of F-18 FDG PET/CT for prediction of microvascular invasion of hepatocellular carcinoma: a meta-analysis. *Clin. Imaging* 79, 251–258. doi:10.1016/j.clinimag.2021.06.015

Kim, Y. I., Kim, Y. J., Paeng, J. C., Cheon, G. J., Lee, D. S., Chung, J. K., et al. (2017). Prediction of breast cancer recurrence using lymph node metabolic and volumetric parameters from 18F-FDG PET/CT in operable triple-negative breast cancer. *Eur. J. Nucl. Med. Mol. Imaging* 44 (11), 1787–1795. doi:10.1007/s00259-017-3748-7

Kornberg, A., Freesmeyer, M., Bärthel, E., Jandt, K., Katenkamp, K., Steenbeck, J., et al. (2009). 18F-FDG-uptake of hepatocellular carcinoma on PET predicts microvascular tumor invasion in liver transplant patients. *Am. J. Transpl.* 9, 592–600. doi:10.1111/j.1600-6143.2008.02516.x

Lee, J. W., Paeng, J. C., Kang, K. W., Kwon, H. W., Suh, K. S., Chung, J. K., et al. (2009). Prediction of tumor recurrence by 18F-FDG PET in liver transplantation for hepatocellular carcinoma. *J. Nucl. Med.* 50, 682–687. doi:10.2967/jnumed.108.060574

Li, Y., Zhang, Y., Fang, Q., Zhang, X., Hou, P., Wu, H., et al. (2021). Radiomics analysis of [18F] FDG PET/CT for microvascular invasion and prognosis prediction in very-early- and early-stage hepatocellular carcinoma. *Eur. J. Nucl. Med. Mol. Imaging* 48, 2599–2614. doi:10.1007/s00259-020-05119-9

Lin, C. Y., Liao, C. W., Chu, L. Y., Yen, K. Y., Jeng, L. B., Hsu, C. N., et al. (2017). Predictive value of 18F-FDG PET/CT for vascular invasion in patients with hepatocellular carcinoma before liver transplantation. *Clin. Nucl. Med.* 42, e183. doi:10.1097/RLU.0000000000001545

- Lin, D. C., Mayakonda, A., Dinh, H. Q., Huang, P., Lin, L., Liu, X., et al. (2017). Genomic and epigenomic heterogeneity of hepatocellular carcinoma. *Cancer Res.* 77, 2255–2265. doi:10.1158/0008-5472.CAN-16-2822
- Lu, L. C., Hsu, C. H., Hsu, C., and Cheng, A. L. (2016). Tumor heterogeneity in hepatocellular carcinoma: facing the challenges. *Liver Cancer* 5, 128–138. doi:10.1159/000367754
- Meng, X. P., Wang, Y. C., Zhou, J. Y., Yu, Q., Lu, C. Q., Xia, C., et al. (2021). Comparison of MRI and CT for the prediction of microvascular invasion in solitary hepatocellular carcinoma based on a non-radiomics and radiomics method: which imaging modality is better? *J. Magn. Reson. Imaging* 54, 526–536. doi:10.1002/jmri.27575
- Miyata, R., Tanimoto, A., Wakabayashi, G., Shimazu, M., Nakatsuka, S., Mukai, M., et al. (2006). Accuracy of preoperative prediction of microinvasion of portal vein in hepatocellular carcinoma using superparamagnetic iron oxide-enhanced magnetic resonance imaging and computed tomography during hepatic angiography. *J. Gastroenterol.* 41, 987–995. doi:10.1007/s00535-006-1890-2
- Mlynarsky, L., Menachem, Y., and Shibolet, O. (2015). Treatment of hepatocellular carcinoma: steps forward but still a long way to go. *World J. Hepatol.* 7, 566–574. doi:10.4254/wjh.v7.i3.566
- Mulé, S., Chalaye, J., Legou, F., Tenenhaus, A., Calderaro, J., Galletto Pregliasco, A., et al. (2020). Hepatobiliary MR contrast agent uptake as a predictive biomarker of aggressive features on pathology and reduced recurrence-free survival in resectable hepatocellular carcinoma: comparison with dual-tracer 18F-FDG and 18F-fch PET/CT. *Eur. Radiol.* 30, 5348–5357. doi:10.1007/s00330-020-06923-5
- Nakashima, Y., Nakashima, O., Tanaka, M., Okuda, K., Nakashima, M., Kojiro, M., et al. (2003). Portal vein invasion and intrahepatic micrometastasis in small hepatocellular carcinoma by gross type. *Hepatol. Res.* 26, 142–147. doi:10.1016/s1386-6346(03)00007-x
- Nishie, A., Yoshimitsu, K., Asayama, Y., Irie, H., Tajima, T., Hirakawa, M., et al. (2008). Radiologic detectability of minute portal venous invasion in hepatocellular carcinoma. *AJR. Am. J. Roentgenol.* 190, 81–87. doi:10.2214/AJR.07.2810
- Ochiai, T., Ikoma, H., Okamoto, K., Kokuba, Y., Sonoyama, T., Otsuji, E., et al. (2012). Clinicopathologic features and risk factors for extrahepatic recurrences of hepatocellular carcinoma after curative resection. *World J. Surg.* 36, 136–143. doi:10.1007/s00268-011-1317-y
- Pinker, K., Shitano, F., Sala, E., Do, R. K., Young, R. J., Wibmer, A. G., et al. (2018). Background, current role, and potential applications of radiogenomics. *J. Magn. Reson. Imaging* 47, 604–620. doi:10.1002/jmri.25870
- Rhee, H., Cho, E. S., Nahm, J. H., Jang, M., Chung, Y. E., Baek, S., et al. (2021). Gadoteric acid-enhanced MRI of macrotubercular-massive hepatocellular carcinoma and its prognostic implications. *J. Hepatol.* 74, 109–121. doi:10.1016/j.jhep.2020.08.013
- Roayaie, S., Blume, I. N., Thung, S. N., Park, Y. N., Kim, M. J., Kim, K. S., et al. (2009). A system of classifying microvascular invasion to predict outcome after resection in patients with hepatocellular carcinoma. *Gastroenterology* 137, 850–855. doi:10.1053/j.gastro.2009.06.003
- Segal, E., Sirlin, C. B., Ooi, C., Adler, A. S., Gollub, J., Chen, X., et al. (2007). Decoding global gene expression programs in liver cancer by noninvasive imaging. *Nat. Biotechnol.* 25, 675–680. doi:10.1038/nbt1306
- Sung, H., Ferlay, J., Siegel, R. L., Laversanne, M., Soerjomataram, I., Jemal, A., et al. (2021). Global cancer statistics 2020: GLOBOCAN estimates of incidence and mortality worldwide for 36 cancers in 185 countries. *Ca. Cancer J. Clin.* 71, 209–249. doi:10.3322/caac.21660
- Szczypinski, P. M., Strzelecki, M., Materka, A., and Klepaczko, A. (2009). MaZda—a software package for image texture analysis. *Comput. Methods Programs Biomed.* 94, 66–76. doi:10.1016/j.cmpb.2008.08.005
- Tampaki, M., Papatheodoridis, G. V., and Cholongitas, E. (2021). Intrahepatic recurrence of hepatocellular carcinoma after resection: an update. *Clin. J. Gastroenterol.* 14, 699–713. doi:10.1007/s12328-021-01394-7
- Teefey, S. A., Hildeboldt, C. C., Dehdashti, F., Siegel, B. A., Peters, M. G., Heiken, J. P., et al. (2003). Detection of primary hepatic malignancy in liver transplant candidates: prospective comparison of CT, MR imaging, US, and PET. *Radiology* 226, 533–542. doi:10.1148/radiol.2262011980
- Witjes, C. D., Willemsen, F. E., Verheij, J., van der Veer, S. J., Hansen, B. E., Verhoef, C., et al. (2012). Histological differentiation grade and microvascular invasion of hepatocellular carcinoma predicted by dynamic contrast-enhanced MRI. *J. Magn. Reson. Imaging* 36, 641–647. doi:10.1002/jmri.23681
- Xu, X., Zhang, H. L., Liu, Q. P., Sun, S. W., Zhang, J., Zhu, F. P., et al. (2019). Radiomic analysis of contrast-enhanced CT predicts microvascular invasion and outcome in hepatocellular carcinoma. *J. Hepatol.* 70, 1133–1144. doi:10.1016/j.jhep.2019.02.023
- Zhang, L., Yu, X., Wei, W., Pan, X., Lu, L., Xia, J., et al. (2020). Prediction of HCC microvascular invasion with gadobenate-enhanced MRI: correlation with pathology. *Eur. Radiol.* 30, 5327–5336. doi:10.1007/s00330-020-06895-6